ACS APPLIED MATERIALS & INTERFACES

Research Article

www.acsami.org

Strong, Reversible Underwater Adhesion via Gecko-Inspired Hydrophobic Fibers

Babak Soltannia and Dan Sameoto*

Department of Mechanical Engineering, University of Alberta, 4-9, Mechanical Engineering Building, Edmonton, Alberta T6G 2G8, Canada

Supporting Information

ABSTRACT: Strong, reversible underwater adhesion using gecko-inspired surfaces is achievable through the use of a hydrophobic structural material and does not require surface modification or suction cup effects for this adhesion to be effective. Increased surface energy can aid in dry adhesion in an air environment but strongly degrades wet adhesion via reduction of interfacial energy underwater. A direct comparison of structurally identical but chemically different mushroom shaped fibers shows that strong, reversible adhesion, even in a fully wetted, stable state, is feasible underwater if the structural material of the fibers is hydrophobic and the mating surface is not strongly hydrophilic. The exact adhesion strength will be a function of the underwater interfacial energy between surfaces and the specific failure modes of individual fibers. This underwater adhesion has been calculated to be potentially greater than the dry adhesion for specific combinations of hydrophobic surfaces.

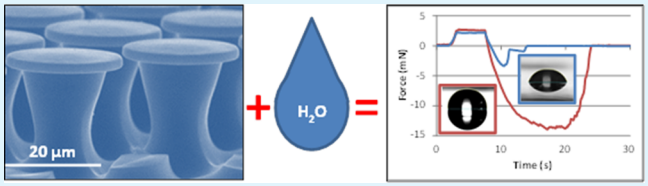

KEYWORDS: *gecko-inspired, dry adhesion, hydrophobic, hydrophilic, underwater*

1. INTRODUCTION

We have developed a direct molding technology for bioinspired dry adhesives that can manufacture identically shaped fibers with a variety of structural elastomers, ranging from hydrophilic polyurethanes to hydrophobic thermoplastic elastomers and silicone rubbers. Testing these materials in air and underwater indicates that underwater performance is strongly reduced for the hydrophilic materials, while it is potentially enhanced in the case of hydrophobic materials. This strong adhesion is achieved without needing special surface treatments or reliance on either suction or capillary interactions for reversible bonding underwater. For over a decade, researchers have been attempting to mimic the extraordinary adhesive capabilities of the gecko, which relies primarily on van der Waals interactions and highly specialized nanostructures on its foot hairs to achieve significant macroscale adhesion. While man-made versions can often outperform their natural inspiration in a few selected applications,[1] natural gecko adhesives have thus far still been proven to be better at interacting with real world environments, such as rough or dirty surfaces. In the case of wet environments, there is a large body of research on synthetic adhesive behavior but with large ranges of performance and occasionally contradictory or inconsistent findings reported.

The major mechanisms by which underwater adhesion can be achieved by geckos or gecko-inspired adhesives include chemical surface modifications to replicate the protein-based underwater adhesives of mussels and similar shellfish, suction based effects due to the wide tipped geometry of specific fibers, air-trapping and capillary interactions between fibers and a supporting surface, hydrophobic−hydrophobic interactions, and direct van der Waals interactions. Some researchers have tried to enhance synthetic fibrillar dry adhesives with the addition of mussel inspired proteins which can bond strongly underwater.[2−4] While the initial application of this technology looks promising, the stability of the proteins used in this technique is often lacking, and oxidation in various environments can dramatically degrade performance.[5] This particular adhesion mechanism also does not explain why the natural gecko adhesive still works in relatively wet environments. Strong underwater adhesion using mushroom shaped fibers in the past have been attributed to microscale passive suction cup features,[6,7] where a very compliant cap is able to be detached from a surface while maintaining a pressure differential between the cap and the environment. Such a suction effect is not always seen in mushroom shaped fibers, however,[8] and the ultimate adhesion strength due to a suction mechanism is often smaller than what could be achieved with optimized van der Waals based adhesion.[9] Suction is also dismissed as a primary mechanism by which real geckos adhere while wet because their foot hair structure does not have the geometry to trap air in the same way as mushroom-shaped synthetics. More recently, groups have reported that trapped air bubbles between foot hairs in animals like beetles and geckos can actually result in strong underwater adhesion which is attributed to a complex combination of van der Waals adhesion in the dry areas, pressure differences, and surface tension forces around the perimeter of trapped air bubbles.[10] For these passive trapped bubbles, underwater traction and adhesion of beetles were

Received: July 22, 2014
Accepted: December 2, 2014
Published: December 2, 2014

strongly reduced on hydrophilic surfaces but less affected on hydrophobic surfaces. Similar results are seen for the actual gecko; however, this adhesion mechanism is lost when the foot hairs are fully wetted.[11,12]

Each of the mechanisms proposed for reversible synthetic adhesives for underwater use has challenges associated with them. For instance, tests with DOPA inspired proteins[2−4] often rely on a thin grafted coating which may not necessarily be stable for long-term use, and exact experimental protocols can be challenging to duplicate. The existence of air/water interfaces in some tests[10−12] relies on metastable states and may not be good for long-term performance. Tests on fibrillar adhesives that are completely wetted have reported inconsistent results regarding whether water contact angles are a significant parameter or not affecting adhesion strength. PDMS fibers without an air gap (and with no overhanding caps) had little reported adhesion underwater,[10] but mushroom shaped fibers that are fully wetted have shown improved adhesion underwater compared to air.[7] Another report using a fibrillar design with a full supported hydrophobic membrane (not separate mushroom caps) was tested and showed spontaneous gas trapping and improved adhesion when tested against a hydrophobic surface and little if any adhesion against a hydrophilic surface[13] which implies water contact angle is a significant parameter on underwater adhesion. However, in different work with an alternative structural material, mushroom shaped fibers tested against both hydrophilic and hydrophobic surfaces were reported to show negligible performance difference underwater.[7] The paper that showed high adhesion underwater with mushroom shaped fibers (and negligible differences between hydrophilic and hydrophobic surfaces) used a flat glass contact with a disk of fibers and pulled off at relatively high speeds (100 μm/s)[7] which potentially could have resulted in a partial suction cup effect through fluidic resistance between the fibers and may have been similar to Stefan adhesion.[14] More recent work with the same fibers, using a hemispherical sapphire indenter found that fully wetted adhesion was worse, and in contrast the adhesion with a trapped air film was better than performance in air[15] when pulled off at 200 μm/s. The hemispherical probe may have had less of an impact on generating similar phenomenon to Stefan adhesion, and thus, the adhesion then became sensitive to contact angles and wettability as suction might not have been as influential.

Ideally, an adhesive that works underwater could be developed without requiring either metastable states or chemically unstable surface treatments and could maintain a significant percentage of its in-air adhesion (or possibly exceed it). Our hypothesis based on the reported literature is that mushroom shaped gecko-inspired adhesives should be possible to operate underwater if they rely on interfacial energy directly which is feasible for hydrophobic materials. What we report for the first time is the direct comparison of several mushroom-shaped polymer arrays with identical fiber geometry operated in air and underwater. No special preparations or surface treatments are completed so that only the baseline polymers are compared for their applicability for use in wet environments. One of these polymers is slightly hydrophilic while the other two are slightly hydrophobic and highly hydrophobic, and because of this change in contact angle with water, we see a dramatic relative difference in adhesion performance when wet, with the hydrophobic fibers outperforming the hydrophilic designs even when in contact with a relatively hydrophilic ruby or sapphire contact surface. Additionally, we initially test these fibers both with a thin air film trapped (plastron film) and after a vacuum degas of the water to fully wet the fibers and observe very small performance differences for the hydrophobic polymer between the wetted conditions (degassed and nondegassed). We thus conclude that it is feasible for identically patterned geometries of gecko-inspired adhesives to maintain strong adhesion compared to their dry performance in wet environments, without taking advantage of surface treatments or metastable wetting states so long as the contact materials are not excessively hydrophilic.

2. FABRICATION AND TESTING

Both structured and unstructured surfaces are manufactured in a variation of a process described elsewhere.[16−18] A master mold made of acrylic and SU-8 is replicated first in a negative silicone rubber mold, followed by a second replica to produce the original structures manufactured from acrylic/SU-8 in the final structural polymer. ST-1060 polyurethane from BJB Enterprises ($E \approx 2.9$ MPa [19]), G1657 from Kraton Performance Plastics ($E \approx 2.4$ MPa [19]), and Sylgard 184 polydimethylsiloxane (PDMS, $E \approx 2.6$ MPa [20]) from Dow Corning were purchased for manufacturing these fibers from the negative silicone molds. ST-1060 is a curable elastomer and was mixed according to the manufacturers' recommended ratios, poured on the silicone molds, and degassed for 30 min. After degassing it was cured at room temperature for 24 h followed by postcuring while still in the silicone mold for several days at 80 °C. G1657 pellets were first melted into a puck on a hot plate before being thermocompression-molded into a silicone mold while supported by a glass microscope slide. The micromolding process used a Branson ultrasonic welder (2000X f/aef) with no ultrasonic energy applied to provide constant force on the puck while it was held at 200 °C on a hot plate for 30 s. After molding was complete, the glass slide, mold, and G1657 were cooled to room temperature (∼1 min) before careful demolding to ensure the elastomer stayed fully on the supporting glass slide. For Sylgard 184, a TC-5030 mold was first activated with oxygen plasma and then silanized with trichloro(1*H*,1*H*,2*H*,2*H*-perfluorooctyl)silane to ensure that the PDMS would not adhere to the TC-5030 mold. The Sylgard was mixed at a ratio of 10:1 of base to cross-linking agent, poured on the mold, and degassed for 30 min followed by curing at 50 °C for 48 h before demolding. After demolding, the Sylgard 184 was postcured for 30 min at 150 °C to improve strength and mechanical properties. The backing layer thickness of the samples is at least 1 mm unless specified to reduce the influence of the stiff glass slide support. The PDMS sample was approximately 2 mm thick because of the casting process (it was cured directly between the TC-5030 mold and a Petri dish) and requirements to demold it without tearing from the silanized mold.

The adhesives were bonded to a glass slide (directly in the case of the G1657 or with a double sided adhesive in the case of ST-1060) and placed in a polystyrene Petri-dish lid. The adhesion test setup is the same as described previously,[16] with two major changes: all tests were done within a Petri dish lid to contain water for wet tests, and the indenter was either a colorless sapphire (Al_2O_3) or ruby (chromium doped sapphire) hemisphere of 6 mm diameter. The test system consisted of a GSO-25 load cell (Transducer Techniques) with a 6 mm diameter sapphire hemisphere (Edmund Optics no. 49-556) or ruby hemisphere (Edmund Optics no. 49-565) for improved

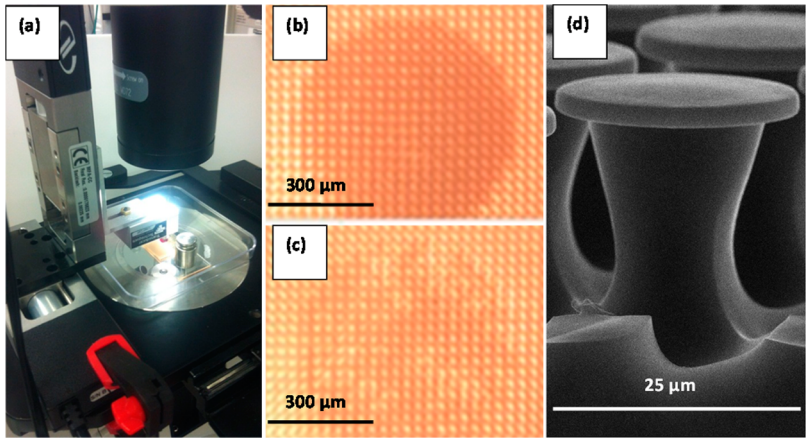

Figure 1. (a) Picture of test system including ruby indenter. Contact area of G1657 thermoplastic elastomer at 30 mN preload (b) and during pull-off (c) in air. SEM of the fibers used is shown in (d).

visibility of contact area. The force probe was positioned by two MFA-CC linear stages (Newport), and normal adhesion data were recorded by custom LabView software. Calibration of the probe was completed immediately prior to testing, and zeroing out of the buoyancy force of the probe tip was completed just before contact with the surface so as to not significantly influence the measurements. The adhesion test system was placed on an inverted microscope so that observations of the contact area could be completed, although only in ambient air was the image quality good enough to directly see the area in contact. The lower difference in index of refraction between the water and the fibers combined with the rounded fiber base (and light scattering) meant direct contact areas in the underwater trials could not be adequately observed even with the ruby tip. Trials were first completed in ambient air, followed by pouring DI water into the Petri dish while the slide was held in place by weights. Tests were completed on fibers with a trapped air film where possible, and then the Petri dish with water was transferred to a vacuum oven and degassed for several minutes at less than 0.5 psi (i.e., water was boiling at room temperature) before venting, which permitted the water to fill in all gaps between fibers for final testing. Any remaining bubbles pinned to the fiber arrays were removed with a pipet before completing degassed trials.

We compare relative magnitudes of pull-off force for various preload conditions as a metric to compare structured and unstructured hydrophobic and hydrophilic polymers in both air and water. To keep comparisons simple, all tests are completed at the same approach and pull-off velocity (5 μm/s), and preloads are held for 3 s each before pull-off. The air temperature in the lab was kept consistent at approximately 22 ± 1 °C, and it is assumed that the mechanical properties of the polymers are not significantly altered by the exposure to water at these temperatures. Figure 1 shows contact area views and SEM images of the fiber designs that were tested in this work. The fibers had a 24 μm diameter cap, 2 μm thick that was overhanging the supporting fiber by 3 μm. The approximate total fiber height was 25 μm and had a minimum cross section at the neck of ~11 μm × 11 μm which was approximately square shaped because of the proximity effects of the caps on the uncollimated exposure.

ST-1060 is slightly hydrophilic (reported water contact angle of 82° [21]), and other SEBS elastomers have a reported water contact angle of approximately 102°,[22,23] making them hydrophobic. Sylgard 184 has been extensively studied in the literature and can have a high range of reported contact angles, up to nearly 120°. Sapphire has been reported to be hydrophilic but with papers reporting very different values for contact angle with water, ~53° [24] and ~85°.[25] To get more accurate values for our own process and equipment, water contact angles were measured on flat surfaces of ST-1060, SEBS, and Sylgard 184 and on pristine hemispherical indenters of ruby and sapphire with a First Ten Angstroms FTA135 system. The results for contact angle measurements (minimum of six trials for flat surfaces and four trails for hemispheres) are listed in Table 1.

Table 1. Contact Angle Measurements for Water on Various Surfaces Used in These Experiments

ST-1060	G1657	Sylgard 184	sapphire	ruby
77 ± 6°	94 ± 3.5°	103 ± 1°	52 ± 6°	61 ± 8°

Flat surfaces were measured using the 10 Å system software, while contact angles on ruby and sapphire had to be measured using National Instruments Vision Builder software from raw images taken with the FTA135. Higher errors were introduced to the rounded surfaces because of droplet sliding if more than 1 μL was used and the resulting small droplets and image pixilation made angle accuracy no better than 5°.

Preloads from 2 to 30 mN were applied, and maximum adhesion was recorded for fibers in ambient dry environments, in DI water with a native trapped air film (plastron), and in DI water after degassing to eliminate the plastron. Comparisons of adhesion forces are made between samples with the same nominal preloads to determine the general effects of different structural and tip materials when tested in air, with air trapped underwater, and when fully wetted.

3. EXPERIMENTAL RESULTS

Tests completed on the hydrophilic and hydrophobic polymers show comparable levels of adhesion vs preload as shown in Figure 2, with slightly higher adhesion of the ST-1060 at any given preload when tested in air, similar to our previously reported results with lower aspect ratio fibers.[17] The average adhesion strength (pull-off force divided by the projected circular contact area) at 2 mN was ~80 kPa for Sylgard 184, ~165 kPa for G1657, and ~245 kPa for the ST-1060 fibers. The adhesion pressure measured for hemispherical indenters is highest with lower preloads,[26] so the lowest of our preloads was used to calculate this value. This is a conservative estimate of adhesion

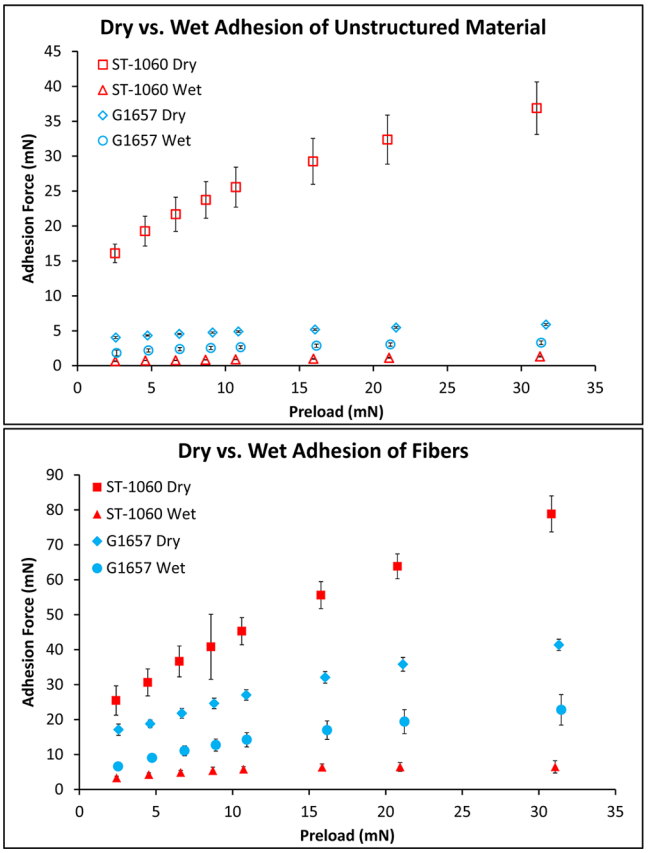

Figure 2. Wet vs dry performance of ST-1060 and G1657 unstructured and structured surfaces as measured with a sapphire hemisphere.

strength, as it does not consider that the actual contact area of fibers is less (~50%). The contact area of Sylgard 184 was greater by approximately 35% at 2 mN because of the larger backing layer thickness.

When compared in their unstructured form, the overall adhesion force of ST-1060 is shown to be higher in air than the G1657 or Sylgard 184 but dramatically loses strength when wet, while the G1657 and Sylgard 184 show less relative adhesion loss underwater. One complicating feature is that the large flat areas had more unevenness and small defects on the G1657 replica, and for the smaller preloads there were more sections with trapped water at the interface. This effect is also observed on fibers, where failure does not always occur at the perimeter of the contact area first (as seen in Figure 1b), indicating local flaws in random fibers. For the fibers, the trends are similar, with the ST-1060 out-performing in a dry environment but losing most adhesion while underwater as the fibers are quickly wetted once preload is applied. Qualitatively, there was a lot more location variability of the ST-1060 adhesion, which could possibly be attributed to slight changes in surface energy in different locations, and the ST-1060 had the greatest variation in measured contact angles. Given that the material is only slightly hydrophilic, there may be areas where residual silicone contamination from the molding process[21] makes it more hydrophobic and thus variable in adhesion strength on the microscale when wet. A comparison of the ST-1060 and G1657 samples with approximately the same backing layer is shown in Figure 2.

In contrast to the much worse wet performance of ST-1060, the G1657 fibers lose only approximately 50% of their adhesion strength when operated with the air−film mostly intact or after degassing. Over the course of 3+ hours during the underwater trials, approximately half of the air trapped between fibers is expelled into larger bubbles that then become pinned to the fiber surface (shown in Figure 3), but the adhesion appeared relatively consistent despite this occurrence.

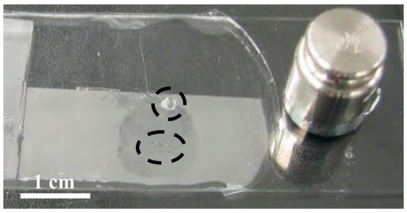

Figure 3. Picture of a G1657 adhesive design after testing with air film trapped. The top circle shows a large air bubble that coalesced after partial wetting occurred around the areas under test (shown approximately with the ellipse). Partial wetting occurred in an area approximately 1 cm in diameter.

Another trial that was completed in an attempt to reduce the surface defects occasionally seen on the thick samples of G1657 was to mold the material at higher force, resulting in a thinner backing layer but fewer surface defects. It is not directly compared to the ST-1060 trials because of possible influence from the supporting glass (the backing layer is only ~200 μm thick) but unlike the thick G1657 sample, this version actually shows improved adhesion underwater compared to air for both the cases of unstructured and structured materials as shown in Figure 4.

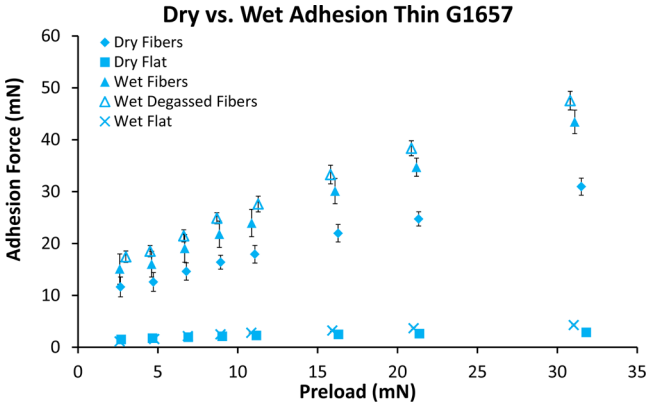

Figure 4. Wet vs dry performance of thin G1657 unstructured and structured surfaces with a very thin (~200 μm) backing layer thickness.

The suspected reason for this improvement is related to the change in type of pull-off event from a multipeak pull-off to a more standard single maximum event, as elaborated in the next section. The multipeak pull-off events tended to occur more often in our tests if the backing layer was very thin because highly uneven loads in the fibers would result because of the spherical indentation geometry. The perimeter of the contact area experienced both higher tensile loads and more torsional loads than the center fibers. There was less change in adhesion for the unstructured material underwater in this trial, however, which by itself was an improvement over the thicker G1657 samples.

The performance of the fully wetted G1657 fibers is nearly identical to the case where there is a thin air film trapped (in some cases superior as seen in Figure 4), contrary to our initial expectations that a plastron may substantially improve performance. This leads to the conclusion that capillary interactions, suction, or other effects related to an air/water interface are far less important than the native van der Waals adhesion for these hydrophobic fibers. The results demonstrate that if a hydrophobic material is chosen for the dry adhesive structural material and enough preload is applied to permit the surfaces to come in contact, the structured material can be nearly as strong while wet as it is dry, despite being in contact with a relatively hydrophilic matching surface. Others have noted the effect of hydrophobic interactions permitting water molecules to be expelled from between surfaces and

significant work of adhesion underwater between hydrophobic surfaces.[13] Where a surface is highly wetted however by water, this interaction would not be feasible, as bonds between the surface and water molecules might be too high to overcome and no true surface contact could occur, thus preventing underwater adhesion.[13]

Our last experiment was designed to confirm this hypothesis without the complication of having a very thin backing layer. The Sylgard 184 replicas from a silanized TC-5030 mold were placed on glass slides as before and tested in air and after degassing. The resulting performance for Sylgard 184 is shown in Figure 5.

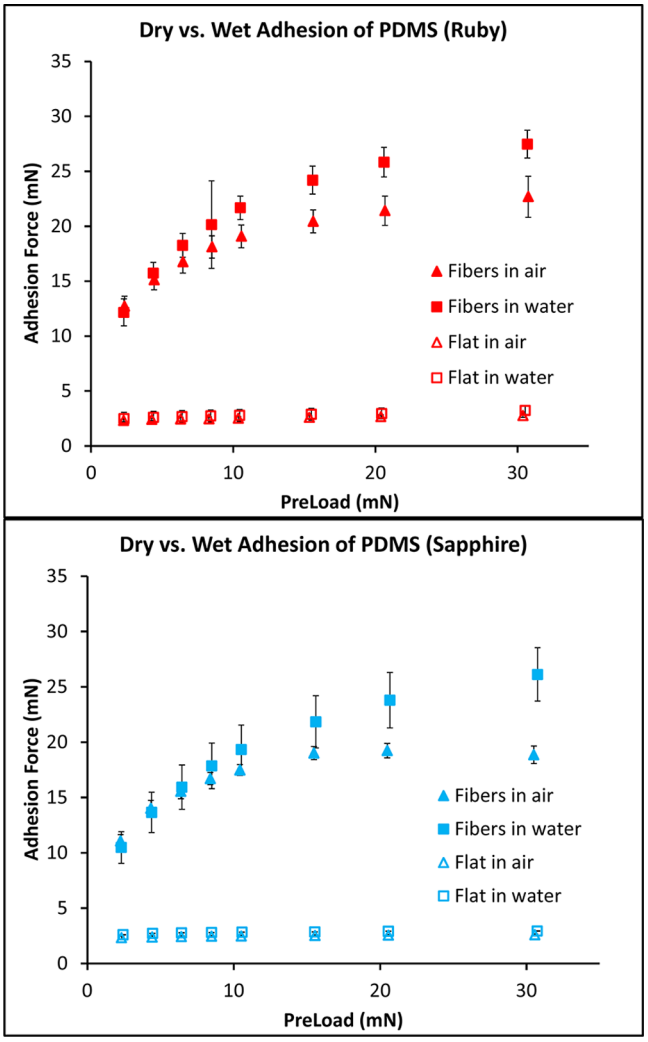

Figure 5. Wet vs dry performance of Sylgard 184 (PDMS) fibers in air and underwater for ruby and sapphire indenters (backing layer is approximately 2 mm thick). Underwater adhesion is improved in both cases compared to in-air performance at higher preloads for fibers, but little difference is observed for flat materials or with low preloads on fibers.

As a metric to compare the ratios of performance of the wetted materials to their dry operation, the pull-off force at each nominal preload in the degassed wetted and dry cases was averaged and compared. The ratios, along with the variability in those ratios, are plotted in Figure 6. The most hydrophilic samples have strongly reduced wet adhesion compared to their dry performance, and the most hydrophobic material (Sylgard 184) actually has improved performance. The underwater performance is extremely sensitive to small surface energy and water contact angle differences, and the average contact angle measured on the ruby indenter was higher on average than the sapphire which appears consistent with the trends

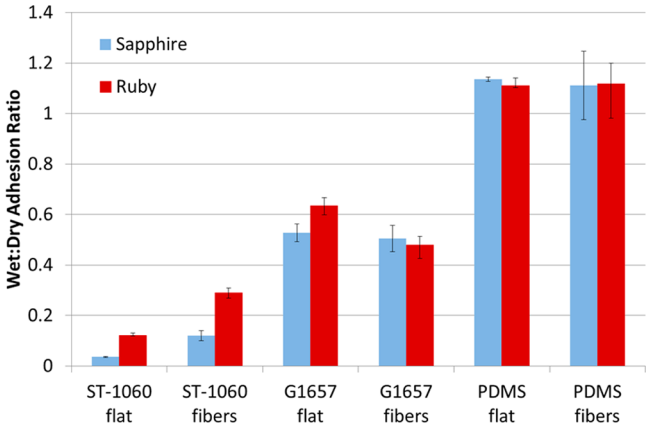

Figure 6. Calculated average wet:dry adhesion ratios for each nominal preload of thick samples in fully wetted and dry conditions.

observed with ST-1060 structural materials. Far more trials and more accurate contact angle measurements would likely be needed in future to provide higher confidence that this effect is real and not a side effect of hydrophobic contamination on the ST-1060.

4. DISCUSSION AND THEORY

Hydrophobic interactions have been proposed to increase the underwater adhesion force of natural gecko setae,[27] but the exact mechanisms by which this occurs have not been fully described. With high precision instruments like a surface force apparatus (SFA), or atomic force microscope (AFM), attraction between hydrophobic surfaces underwater has been observed on length scales up to several hundred nanometers.[28] In these cases, the presence of nanobubbles or other effects from dissolved gases in the liquid appears to be primarily responsible, as the distance and magnitude that these forces act at are strongly reduced by removal of dissolved gases through deaeration. Even after deaeration what sometimes happens is that hydrophobic surfaces will "jump" into contact with one another underwater at longer ranges than may otherwise be expected, but once in contact direct molecular interactions will hold the surfaces in place. While our test system is not sensitive enough to observe this jump-in effect at tens to hundreds of nanometers, the natural and spontaneous expulsion/vaporization of water from between hydrophobic surfaces in close proximity may be analogous to capillary condensation in hydrophilic surfaces.[28] For dissimilar materials, if the combined contact angle between two surfaces is greater than 180°, it has been observed for both capillary filling[29] and capillary adhesion[30] that the combined surfaces will act as a hydrophobic−hydrophobic interface. The modes of adhesion failure will determine whether surface−liquid or surface−gas/vacuum interfacial energies should be used to calculate adhesion strength.

To help better understand our experimental results, we apply the methods and models recently proposed in other work. Stark et al.[11] describe several mechanisms of real gecko adhesion underwater as well as how surface wettability will influence the ultimate adhesion. While the actual tests they run underwater are looking primarily at shear adhesion, they derive a model to predict ratio of in-air to underwater adhesion that is based on normal adhesion assumptions. We look specifically at the case where the gecko fibers are assumed to be fully wetted underwater before and after contact with an opposing surface (to match our degassed fiber case) and compare this predicted

adhesion ratio to our findings. The general form of the work of adhesion between two surfaces is written as

$$W_{dry} = A_c(\gamma_1 + \gamma_2 - \gamma_{1-2}) \quad (1)$$

where W_{dry} is the work of adhesion between the surfaces, A_c is the area in contact, γ_1 and γ_2 are the free surface energies of each surface, and γ_{1-2} is the interfacial energy of the contact between the surfaces. When operated dry, the equation can be rewritten as

$$W_{dry} = A_c(\gamma_{s-air} + \gamma_{f-air} - \gamma_{s-f}) \quad (2)$$

where the energies between the surface and fiber and interfacial energies of contact between the fiber and surface materials are substituted. Because most of the individual components of surface energy are not known, Stark et al. use the surface interactions between a proxy solvent (*n*-hexadecane) that represents the lipids known to be on gecko foot hairs to substitute for the surface fiber interaction. If we were to perform a similar substitution, W_{dry} could be written as

$$W_{dry} = A_c(\gamma_{f-air}(1 + \cos\theta_1)) \quad (3)$$

where θ_1 would represent the contact angle of *n*-hexadecane on the contact surface. If our fibers were made of or coated with the same material, such a substitution could provide more details on exactly what adhesive strength could be expected. In our case, however, we will use it as a convenient proxy by which to examine the effect of different surface energies in air and water on underwater adhesion. Continuing with the analysis to find the work of underwater adhesion, a similar calculation is performed but in a water medium:

$$W_{wet} = A_c(\gamma_{s-water} + \gamma_{f-water} - \gamma_{s-f}) \quad (4)$$

The interaction energy between a surface and water can be found simply as

$$\gamma_{s-water} = \gamma_{s-air} - \gamma_{water-air}\cos\theta_2 \quad (5)$$

where $\gamma_{water-air}$ is the surface tension of water (~72.8 mN/m) and θ_2 is the water contact angle with the surface material. The complete ratio of wet to dry adhesion assuming a fully wetted condition before and after contact is thus

$$\frac{W_{wet}}{W_{dry}} = \frac{\gamma_{f-water} + \gamma_{f-air}\cos\theta_1 - \gamma_{water-air}\cos\theta_2}{\gamma_{f-air}(1 + \cos\theta_1)} \quad (6)$$

The contact area is canceled out of the equation in this scenario, and we are left with a ratio based on the surface energies of the fiber material and the contact angles of hexadecane and water on the opposing surface. Using an assumed surface energy in air and water contact angle for the fiber materials allows values of wet:dry adhesion to be predicted for a variety of wettability of opposing substrates in Figure 7 and Figure 8. What can be seen in both figures is that the wet:dry adhesion ratio is relatively insensitive to the hexadecane contact angle on the opposing surfaces but is a strong function of the exact contact angle with water. The contact angle limits were selected primarily because they were found in this range for hexadecane on Teflon,[11] and the general limit of water contact angles on unstructured hydrophobic surfaces is approximately 120°.[31] A crossover point between adhesion enhancement and reduction occurs at 86° for SEBS assuming a fully wetting case (0° contact angle) with hexadecane and 103° for ST-1060 with the same assumptions, exactly as is expected

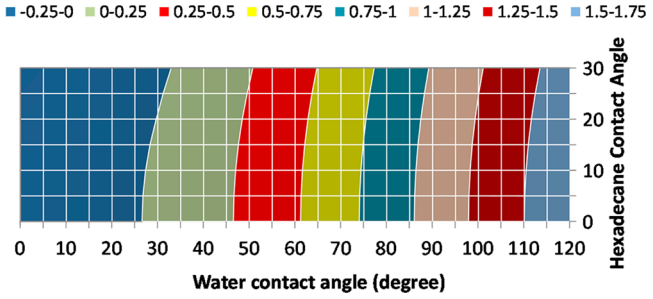

Figure 7. Calculated average wet:dry adhesion ratios for SEBS fibers (γ_{f-air} = 30 mN/m, θ_{2-SEBS} = 94°, $\gamma_{f-water}$ = 35.1 mN/m) for a variety of potential contact angles on an opposing surface.

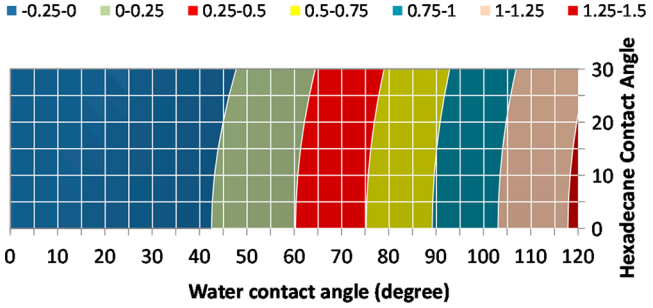

Figure 8. Calculated average wet:dry adhesion ratios for ST-1060 fibers: assumed surface energy in air 35 mN/m, water contact angle with ST-1060 = 77° → underwater interfacial energy = 18.6 mN/m.

when observing a crossover ratio between net hydrophilic or hydrophobic reactions with asymmetric surfaces.[29,30] We note that these ratios actually predict negative values (repulsive forces) for specific low water contact angle cases which may not be matched in reality but would possibly indicate spontaneous release if the surfaces were previously in contact before water was applied.

On the basis of this simple model, it appears likely that for underwater adhesion, a hydrophobic structural material as fibers and a hydrophobic contact surface would be ideal. The total adhesion strength is a strong function of water contact angle on each surface. It can be safely assumed then that local surface energy changes or contamination of the liquid itself via addition of a surfactant or other miscible materials would strongly influence the response. As a general prediction, applied to the unstructured materials, we would normally expect for the contact angles measured on each surface that the adhesion of ST-1060 to sapphire (assuming contact angle of sapphire to be ~50°) would be ~0−20% that of its in-air values and the G1657 to be 20−40%. While this is not exactly the behavior seen in Figure 6, it broadly predicts the relative performance. The bigger deviation is for PDMS, where the calculated adhesion ratio is close to 24% for assumed surface energy of ~20 mN/m, contact angle of 103°, and underwater interfacial energy of ~36.4 mN/m. The actual calculated adhesion ratios for PDMS are very sensitive to contact angle, and even a 10° change in sapphire contact angle would double the adhesion strength. For this reason, it is likely our measured contact angles are underestimates of the true advancing angles on the surfaces and further experiments will be done to make more accurate comparisons.

Another factor to consider however with this model is that it may not necessarily accurately describe the complete pull-off behavior for the fibers in the case where adhesion is strongly

enhanced (i.e., both fibers and mating surfaces are very hydrophobic). For example, the traditional Johnson–Kendall–Roberts (JKR) adhesion tests (and subsequent adhesion models) will often be similar to those of our hemispherical indenter on a flat surface. In this situation, pull-off occurs from the perimeter of the surfaces in contact, and thus the differential in surface energies as the surrounding fluid comes into contact with separated surfaces is a strong driving factor. In the case of mushroom shaped adhesives, the dominating failure mode for well-designed structures is often an internal cavitation followed by a pull-off after which an internal crack reaches the outside of a fiber.[32] For this failure mode of an individual fiber, the surrounding medium should not influence the pull-off force to the same extent (as no fluid would be found within the newly formed void), and only fibers with defects near the perimeter of the cap or designed to peel-off first from the outside edge of the cap could be enhanced initially by the higher interfacial energies underwater. Some evidence of this can be seen in the particular adhesion behavior of our thinnest G1657 samples. Low total adhesion strength is seen because of a double pull-off event when operated dry, indicating that the fibers on the perimeter of the area of contact fail early on, but the fibers in the center that are loaded more axially maintain contact for a longer time. When overlaid with a degassed underwater sample in Figure 9,

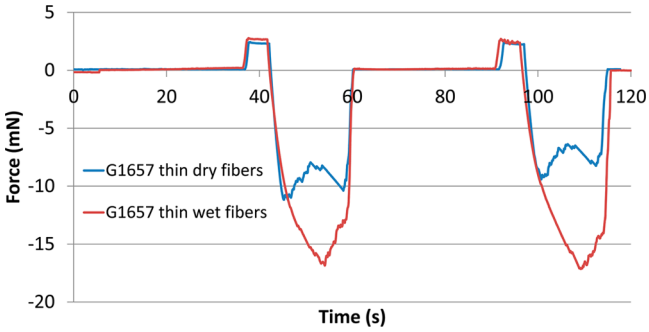

Figure 9. Overlaid real-time data of pull-off events of thin G1657 fibers in air and underwater. Data have been time shifted for clarity. Underwater tests do not delay the removal of the last fibers in contact near the center in this instance but seem to delay the initial peeling from the perimeter of the area in contact.

it is seen that the fibers in the center release after approximately the same time (and thus displacement), but the earlier peeling of the perimeter is significantly delayed. The basic hypothesis of why this behavior occurs is illustrated in Figure 10.

As shown in Figure 10, the fibers in contact with the perimeter of a hemispherical indenter may be more likely to start adhesion failure due to an edge defect because of the extra torque on the caps (particularly noticeable in Figure 9 because of the thin backing layer). In this mode, a higher interfacial energy underwater will improve the adhesion strength of cap edge initiated failures in a manner similar to that in JKR tests. However, for fibers that are loaded axially, the adhesion failure is more likely to be caused by an internal cavitation. If the initial separation of surfaces does not involve any direct exposure to the liquid, the interfacial energy between surfaces in vacuum would still be the dominant factor for determining adhesion strength of these fibers.

Because all of the manufactured caps in this work have a finite fillet at the edge of the cap, if the interfacial adhesion underwater is low (in the case of the contacting surfaces being

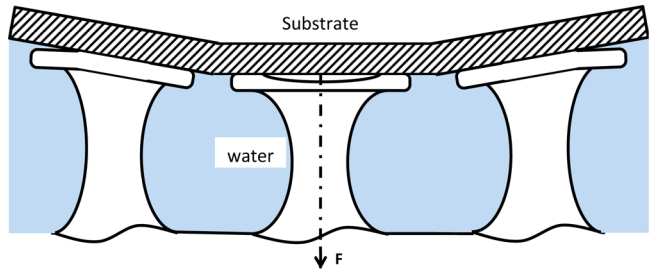

Figure 10. Exaggerated schematic of potential failure modes of mushroom shaped fibers around a hemispherical indenter. In this representation, fibers that have to conform to more angled areas of the indenter are more likely to have an edge initiated failure while those loaded near the center of contact may have an internal cavitation style failure.

hydrophilic), it can reduce adhesion strength of all fibers because lower forces at the perimeter of the caps would be required to initiate a crack. Even for axially loaded mushroom shaped fibers, if the underwater interfacial energy is low enough, then edge initiated failure may occur before the more highly loaded interior. In the extreme case where the combined contact angles are very small the interfacial energy may be negative, which implies a spontaneous loss of adhesion starting at the filleted cap edge without any tensile loads required. The exact point at which a lower interfacial energy will result in an underwater edge initiated failure of a mushroom shaped fiber that normally fails by internal cavitation would have to be predicted with numerical or analytical models similar to those that already determine adhesion failure for defects of known size.[16,32]

5. APPLICATIONS OF FINDINGS

To put these findings into practice, we show that it is feasible to automatically pick up hydrophobic materials from a water bath with a fully wetted G1657 structured adhesive. Microscope coverslips made of glass (Fisherfinest, Premium superslip part no. 12-545-88) or plastic (unbreakable coverslips no. 12-547) are obtained from Fisher Scientific. The glass coverslips are cleaved in two to make squares and then are rinsed with acetone and DI water first to eliminate any surface coatings and make them more hydrophilic. For identification, the back side of the slips is drawn on with a permanent marker. All slips are placed in a polyproplyene container filled with DI water, and a fully wetted G1657 adhesive is pressed lightly on top of the slides before removing from the liquid. As can be seen in Supporting Information video S1, only the hydrophobic plastic cover slips are removed from the water. Similar pressing with the smooth back side of the G1657 resulted in no gripping of any coverslips. Additionally, as expected based on the lower contact angles and higher wettability of solvents like acetone on the surface of these fibers, the application of lower surface tension liquids will reduce or eliminate the adhesion between the G1657 adhesives and other polymers. A polypropylene pipet is shown being removed by acetone from a G1657 adhesive in video S2, and after rinsing with fresh DI water to flush out the lower surface tension acetone, the adhesive can pick up the pipet again even while fully wetted. The loss of adhesion in this case occurs nearly spontaneously because the contact angle of acetone is low enough to make it wick in between adhesive caps and the pipet without needing much extra load beyond the weight of the pipet. Unlike silicone

rubbers and the ST-1060 polyurethane, the G1657 is not dissolved or significantly swelled by acetone or alcohols for these short exposures. Finally, we also tested the adhesive while wet and under lower pressures to demonstrate that there would be little suction component to the adhesive. A polypropylene syringe was filled with weights and suspended with a fully wetted adhesive in water (net weight of ~40g considering buoyancy). The whole structure was degassed in a vacuum oven until water was boiling at room temperature, and despite the significant agitation of the water and sample, no adhesive loss could be observed. This process is shown in video S3.

6. CONCLUSION

Three different elastomers with nearly identical geometry and modulus values but significantly different water contact angles have been used to fabricate mushroom shaped dry adhesives. Testing these materials in air and underwater demonstrates the extreme importance of surface wettability on adhesion performance, where the more hydrophilic a material is, the larger is the reduction in adhesion performance underwater. A simple model for prediction of underwater performance is adapted from other work on interfacial energy and surface wettability for real geckos and shows some broad predictive value in the design of synthetic dry adhesive versions. The ability to achieve reversible, strong adhesion underwater is feasible if structural materials are hydrophobic and they work without specialized surface treatments, capillary forces, suction, or plastrons, potentially making these adhesives more versatile in wet environments. These insights allow controlled adhesion strength through altering surface wettability or surface tension of the surrounding fluid.

■ ASSOCIATED CONTENT

Supporting Information

Three video files showing experimental aspects. This material is available free of charge via the Internet at http://pubs.acs.org.

■ AUTHOR INFORMATION

Corresponding Author

*E-mail: sameoto@ualberta.ca.

Notes

The authors declare no competing financial interest.

■ ACKNOWLEDGMENTS

We thank Brendan Ferguson for his manufacturing of the original molds used in this work. We also acknowledge Hong (Elvis) Sun and Dr. Hongbo Zeng for their early assistance with testing and useful discussions. Finally we thank the editors and reviewers for their constructive comments and suggestions in producing the final manuscript. This work was financially supported by NSERC and Micralyne Inc. under a strategic grants program.

■ REFERENCES

(1) Sameoto, D.; Menon, C. Recent Advances in the Fabrication and Adhesion Testing of Biomimetic Dry Adhesives. *Smart Mater. Struct.* **2010**, *19*, 103001.

(2) Lee, H.; Lee, B. P.; Messersmith, P. B. A Reversible Wet/Dry Adhesive Inspired by Mussels and Geckos. *Nature* **2007**, *448* (7151), 338−341.

(3) Glass, P.; Chung, H.; Washburn, N. R.; Sitti, M. Enhanced Reversible Adhesion of Dopamine Methacrylamide-Coated Elastomer Microfibrillar Structures under Wet Conditions. *Langmuir* **2009**, *25*, 6607−6612.

(4) Glass, P.; Chung, H.; Washburn, N. R.; Sitti, M. Enhanced Wet Adhesion and Shear of Elastomeric Micro-Fiber Arrays with Mushroom Tip Geometry and a Photopolymerized p(DMA-co-MEA) Tip Coating. *Langmuir* **2010**, *26*, 17357−17362.

(5) Anderson, T. H.; Yu, J.; Estrada, A.; Hammer, M. U.; Waite, J. H.; Israelachvili, J. N. The Contribution of DOPA to Substrate−Peptide Adhesion and Internal Cohesion of Mussel-Inspired Synthetic Peptide Films. *Adv. Funct. Mater.* **2010**, *20*, 4196−4205.

(6) Heepe, L.; Varenberg, M.; Itovich, Y.; Gorb, S. N. Suction Component in Adhesion of Mushroom-Shaped Microstructure. *J. R. Soc. Interface* **2011**, *8*, 585−589.

(7) Varenberg, M.; Gorb, S. A Beetle-Inspired Solution for Underwater Adhesion. *J. R. Soc. Interface* **2008**, *5*, 383−385.

(8) Sameoto, D.; Sharif, H.; Menon, C. Investigation of Low-Pressure Adhesion Performance of Mushroom Shaped Biomimetic Dry Adhesives. *J. Adhes. Sci. Technol.* **2012**, *26*, 2641−2652.

(9) Carbone, G.; Pierro, E. Effect of Interfacial Air Entrapment on the Adhesion of Bio-Inspired Mushroom-Shaped Micro-Pillars. *Soft Matter* **2012**, *8*, 7904−7908.

(10) Hosoda, N.; Gorb, S. N. Underwater Locomotion in a Terrestrial Beetle: Bombination of Surface De-Wetting and Capillary Forces. *Proc. R. Soc. B* **2012**, *279*, 4236−4242.

(11) Stark, A. Y.; Badge, I.; Wucinich, N. A.; Sullivan, T. W.; Niewiarowski, P. H.; Dhinojwala, A. Surface Wettability Plays a Significant Role in Gecko Adhesion Underwater. *Proc. Natl. Acad. Sci. U.S.A.* **2013**, *110*, 6340−6345.

(12) Stark, A. Y.; McClung, B.; Niewiarowski, P. H.; Dhinojwala, A. Reduction of Water Surface Tension Significantly Impacts Gecko Adhesion Underwater. *Integr. Comp. Biol.* **2014**, *54*, 1026−1033.

(13) Vajpayee, S.; Jagota, A.; Hui, C. Y. Adhesion of a Fibrillar Interface on Wet and Rough Surfaces. *J. Adhes.* **2010**, *86*, 39−61.

(14) Wainwright, D. K.; Kleinteich, T.; Kleinteich, A.; Gorb, S. N.; Summers, A. P. Stick Tight: Suction Adhesion on Irregular Surfaces in the Northern Clingfish. *Biol. Lett.* **2013**, *9*, 20130234.

(15) Kizilkan, E.; Heepe, L.; Gorb, S. Underwater Adhesion of Mushroom-Shaped Adhesive Microstructure: An Air-entrapment Effect. *Biol. Biomimetic Adhes.* **2013**, 65−71.

(16) Khaled, W. B.; Sameoto, D. Anisotropic Dry Adhesive Via Cap Defects. *Bioinspiration Biomimetics* **2013**, *8*, 044002.

(17) Khaled, W. B.; Sameoto, D. Fabrication and Characterization of Thermoplastic Elastomer Dry Adhesives with High Strength and Low Contamination. *ACS Appl. Mater. Interfaces* **2014**, *6*, 6806−6815.

(18) Sameoto, D.; Menon, C.; Deep, U. V. Patterning of Acrylic Masters for Molding Biomimetic Dry Adhesives. *J. Micromech. Microeng.* **2010**, *20*, 115037.

(19) Bschaden, B. S. *Developing Design Guidelines for Improved Gecko Inspired Dry Adhesive Performance*; University of Alberta: Edmonton, Canada, 2014.

(20) Johnston, I.; McCluskey, D.; Tan, C.; Tracey, M. Mechanical Characterization of Bulk Sylgard 184 for Microfluidics and Micro-engineering. *J. Micromech. Microeng.* **2014**, *24*, 035017.

(21) Kim, S.; Cheung, E.; Sitti, M. Wet Self-Cleaning of Biologically Inspired Elastomer Mushroom Shaped Microfibrillar Adhesives. *Langmuir* **2009**, *25*, 7196−7199.

(22) Martinelli, E.; Agostini, S.; Galli, G.; Chiellini, E.; Glisenti, A.; Pettitt, M. E.; Callow, M. E.; Callow, J. A.; Graf, K.; Bartels, F. W. Nanostructured Films of Amphiphilic Fluorinated Block Copolymers for Fouling Release Application. *Langmuir* **2008**, *24*, 13138−13147.

(23) Xin, Z.; Du, B.; Yan, S.; Du, S.; Ding, J.; Yang, Z.; Ren, W. Surface Modification of Poly(styrene-b-(ethylene-co-butylene)-b-styrene) (SEBS) Elastomer via Covalent Immobilization of Nonionic Sugar-Based Gemini Surfactants. *J. Biomater. Sci., Polym. Ed.* **2014**, *25*, 1−17.

(24) Dai, Z.; Min, Y.; Gorb, S. N. Frictional Characteristics of the Beetle Head-Joint Material. *Wear* **2006**, *260*, 168−174.

(25) Gorb, E.; Hosoda, N.; Miksch, C.; Gorb, S. Slippery Pores: Anti-Adhesive Effect of Nanoporous Substrates on the Beetle Attachment System. *J. R. Soc. Interface* **2010**, rsif20100081.
(26) del Campo, A.; Greiner, C.; Arzt, E. Contact Shape Controls Adhesion of Bioinspired Fibrillar Surfaces. *Langmuir* **2007**, *23*, 10235−10243.
(27) Pesika, N. S.; Zeng, H.; Kristiansen, K.; Zhao, B.; Tian, Y.; Autumn, K.; Israelachvili, J. Gecko Adhesion Pad: A Smart Surface? *J. Phys.: Condens. Matter* **2009**, *21*, 464132.
(28) Meyer, E. E.; Rosenberg, K. J.; Israelachvili, J. Recent Progress in Understanding Hydrophobic Interactions. *Proc. Natl. Acad. Sci. U.S.A.* **2006**, *103*, 15739−15746.
(29) Bullard, J. W.; Garboczi, E. J. Capillary Rise between Planar Surfaces. *Phys. Rev. E: Stat., Nonlinear, Soft Matter Phys.* **2009**, *79*, 011604.
(30) De Souza, E.; Brinkmann, M.; Mohrdieck, C.; Crosby, A.; Arzt, E. Capillary Forces Between Chemically Different Substrates. *Langmuir* **2008**, *24*, 10161−10168.
(31) Nishino, T.; Meguro, M.; Nakamae, K.; Matsushita, M.; Ueda, Y. The Lowest Surface Free Energy Based on $-CF_3$ Alignment. *Langmuir* **1999**, *15*, 4321−4323.
(32) Carbone, G.; Pierro, E. Sticky Bio-Inspired Micropillars: Finding the Best Shape. *Small* **2012**, *8*, 1449−1454.